NORTH SEA OIL PLATFORMS: FAILURE UNDER RANDOM LOADING

R. Foroughi and J. C. Radon

Imperial College of Science and Technology, London SW7 2BX, England

ABSTRACT

A series of fatigue crack growth tests under variable amplitude loading has been conducted on semi-elliptic notched plate specimens made of structural steel BS4360 - 50D, used for offshore oil platform construction. The tests were carried out under pure bending. Two different power spectra, a "broad band" and a "triple-peaked", were chosen for generation of random loading. The effect of thickness, mean stress, band width and power spectrum shape on crack growth rate have been studied.

The results of these tests have shown that resistance to fatigue fracture is independent of thickness within the tested range of 25 to 34 mm. Increases in mean loading stress and band width for a given power spectrum enhance the crack propagation rate. Of the two power spectra examined, the triple-peaked one had an increasing influence on the crack growth rate results.

KEYWORDS

Fatigue crack growth; random loading; semi-elliptical crack; offshore oil platform; mean stress effect.

INTRODUCTION

Constant amplitude (CA) fatigue data have been successfully fitted by a power-law expression (1) of the form:

$$\frac{da}{dN} = C \Delta K^n$$

in the second region (Paris régime) by the application of LEFM. This ordinary differential equation may be used to determine the structural integrity and life estimations of the various engineering components and structures which experience variable-amplitude service loads. However, the outcome of such an analysis is not always accurate due to variation in the fatigue behaviour of materials under random loads. In order to

avoid discrepancies between the service life and the estimated life, components or specimens should be tested under real service load conditions. Unfortunately, this approach may not always be practicable and economically viable, so the tests are carried out under simulated service load conditions.

Parameters inherent in simulated loads influence the fatigue crack growth rate data and such effects magnify under adverse environmental conditions. The influence of mean stress and frequency on crack propagation rates has been studied under CA (3,5,6) and random loading (4,7,8,9). The tests conducted on structural steel under CA loading in air (6) have revealed only a very small mean stress effect and shown that the reduction of frequency enhances growth rate. The fatigue behaviour of two different steels under random loading was also tested in both air and seawater (7,9) and when combined with the reduction of frequency a large mean stress effect was observed.

Geometry changes, such as thickness and size, may also influence crack growth rates. Thickness effects under CA and random load have been examined (6,8). Under variable amplitude loading (8) at low growth rates, the increase in thickness enhances crack growth resistance, while this behaviour is reversed at high growth rates.

Fatigue behaviour also changes as load amplitude variation is introduced (4,8,9). This is due to the load sequence effect. Crack propagation rate differences due to CA and random loads have been examined by Smith (4). His study included the effects of two different power spectra (narrow band and double-peaked-spectrum loads) on the growth rate. It was concluded that at low stress intensity factors, the growth rate caused by random loads was higher than CA results while this effect was reversed at high K values.

To obtain relevant fatigue crack propagation data of structural steel due to simulated loads, the influence of frequency range and power spectrum shape on growth rate must be studied. Mean stress and thickness effects are also significant. The influence of thickness for the range of 12 to 50 mm was examined by Musuva (6). In the tests reported here the range of frequencies within wave loading was between 0 and 0.3 Hz, and the spectral shapes suggested varied from narrow band to double-peaked and broad band (BB) spectra. However, a study of the dynamic response of a North Sea Forties Field platform (10) produced a triple-peaked spectrum which was incorporated into the pseudo-random signal generator developed at Imperial College, London.

The fatigue behaviour of structural steel BS4360 - 50D was investigated under the above spectrum (referred to as the BP spectrum), and also using a broad band signal. The amplitude variation of the two different signals had a normal distribution with zero mean.

EXPERIMENTAL PROCEDURE

Five bend specimens were made from two different thickness plates of structural steel BS4360 - 50D; two of 34 mm and three of 25 mm thick. The yield stress of the material was 388 MPa. (6). The centre of each specimen was notched with a 30° angled cutter. The notch was perpendicular to the rolling direction. The surface notch dimensions are shown in Fig. 1. The specimens were tested under pure bending. The test load system was

the 200 kN closed loop servo-hydraulic machine manufactured by Dartec, UK. All the tests were conducted in air under laboratory conditions at 21°C. A variable amplitude loading was achieved by feeding a filtered signal generated by a pseudo-random signal generator into the external input of the fatigue machine. The signal generator was designed and built at Imperial College. This unit has the versatility of producing a variety of random signals with different power spectra and frequency range. The two spectra used for this study were the broad band and the BP (triple-peaked) spectrum, Fig. 2a. The BP spectrum was developed by analysis of strain measurements made at the British Petroleum Forties Field platform. The BP signal band width was 0.32 Hz. The peaks were at 0.06, 0.18 and 0.28 Hz, respectively. The band width of the broad band (BB) signal was selected at 0.32 and 15 Hz. Samples of these two signals and their spectra are shown in Figs. 2b and 2c.

The test programme plan is shown in Table 1. Fatigue data for each specimen were collected by measurements of major and minor axes of the semi-elliptical surface crack at different time intervals (unit used is seconds).

The surface crack lengths were measured at both tips of the notch by means of a travelling microscope which had a resolution of 0.01 mm. The crack depth measurements were made by use of an AC potential drop crack micro-gauge unit built by the Unit Inspection Company, UK. The depth calculated for the growth rate and stress intensity factor evaluations was obtained by one-dimensional interpretation of voltage measurements across the crack mouth.

All specimens were loaded to an equal mean bending stress, $\bar{\sigma}$, and rms (root mean square) of surface bend stress, σ_{rms}, apart from the last specimen (S5) which was loaded with a smaller $\bar{\sigma}$. This specimen was used for the mean stress effect study. The Q factor ($Q = \bar{\sigma}/\sigma_{rms}$) for all specimens was 12, apart from specimen S5 for which Q was 8.

RESULTS AND DISCUSSION

The crack length and depth measurements were used to calculate the stress intensity factors and growth rates at the respective crack tips. The secant method was applied for the growth rate evaluations. The crack propagation rates were plotted versus the corresponding rms of the stress intensity factors, K_{rms}, on a log-log scale. K_{rms} values are more common and simpler to calculate than the weighted average range of the stress intensity factor suggested in (7,8,9).

Various stress intensity factor solutions for semi-elliptical surface cracked plates under pure bending have been proposed. Scott et al. (2) have reviewed and compared these solutions and concluded that the Koterazawa and Minamisaka solution using the width correction factors developed by Holdbrook and Dover provides the closest results when compared with experimental data. These solutions for the crack depth, a, and the surface crack length, c, Fig. 1., are given by:

$$K_a = \sigma_b M_f(\tfrac{\pi}{2}) M_a M_W \sqrt{\pi a}/E(K)$$

$$K_c = \sigma_b M_f(0) M_c M_W \sqrt{\pi a}/E(K)$$

where σ_b is the surface bend stress.

$$M_f(\tfrac{\pi}{2}) = 1 + 0.12\,(1 - \tfrac{a}{2c})^2$$

$$M_a = 1 - 1.36\,(\tfrac{a}{B})\,(\tfrac{a}{c})^{0.1}$$

$$M_f(0)\,M_c = M_{fc}$$

$$M_{fc} = (M_1\,(1 - 0.3\,(\tfrac{a}{B}))\,\,(1 - (\tfrac{a}{B})^{12}) + 0.394\,E(K)\,(\tfrac{a}{B})^{12}\sqrt{c/a}$$

$$M_1 = (1.21 - 0.1\,(\tfrac{a}{c}) + 0.1\,(\tfrac{a}{c})^4)\,\sqrt{a/c}$$

$$E(K) = (1 + 1.47\,(\tfrac{a}{c})^{1.64})^{\frac{1}{2}}$$

$$M_W = 1 + \frac{f(\frac{a}{c})\,G(\frac{c}{W})\,H(\frac{a}{B})}{(0.2745)^2}$$

$$f(\tfrac{a}{c}) = 0.381 - 0.141\,(\tfrac{a}{c}) - 0.366\,(\tfrac{a}{c})^2 + 0.569\,(\tfrac{a}{c})^3 - 0.248\,(\tfrac{a}{c})^4$$

$$G(\tfrac{c}{W}) = -0.0239 + 1.434\,(\tfrac{c}{W}) - 2.984\,(\tfrac{c}{W})^2 + 7.822\,(\tfrac{c}{W})^3$$

$$H(\tfrac{a}{B}) = -0.0113 + 0.323\,(\tfrac{a}{B}) + 0.749\,(\tfrac{a}{B})^2 - 0.535\,(\tfrac{a}{B})^3$$

The K_{rms} is calculated from the above expressions by replacing σ_b with σ_{rms}.

To examine the influence of thickness on the crack growth rate, the fatigue data of specimens S1 and S2 were compared. Specimen S1 was 25 mm thick and S2 34 mm thick. The notch size was identical for the two specimens. Due to the change of thickness, the stress intensity factor distributions were different for the two specimens. This effect is depicted in Fig. 3 which is a plot of the K_{rms} versus crack dimensions. The stress intensity factors at the depth and at the surface tips of a semi-elliptical crack are functions of thickness and width, as well as of the crack geometry. K at the surface tips is more sensitive to crack geometry change than K at depth. At the same time, the increase in the crack depth influences the K values more significantly than the surface length. These effects were clearly duplicated for the two specimens. However, the K distribution for the thicker specimen had a second effect. After precracking, although K values at the surface tips for the two specimens were identical, the K at depth, K_a, for the thicker specimen was much higher than K at the surface, K_c. This K_a remained predominantly higher than K_c for a large part of crack propagation. The K distribution curves of the S2 specimen crossed each other at the surface length, which was about 36% higher than the length where the thinner specimen K-curves

crossed. The appropriate change of the specimen geometry, such as the increase of the width and notch dimensions of the thicker specimen by 36% of the corresponding dimensions of the thinner specimen, would result in the same K distribution for the two specimens. However, in this test the thickness of S2 was 36% larger than S1 and the width was reduced by 17%.

Despite the K distribution differences present for the two specimens, the crack propagation data correlated well. This is illustrated in Fig. 4 which is a log-log plot of the growth rate versus corresponding K_{rms} at depth and at the surface tips of the cracks. The surface growth rates have coincided but there is a degree of drift present in the depth results of the thicker specimen. However, this effect was expected, as the K_a was larger for specimen S2. The data also depict the fatigue behaviour during the transition into the Paris régime. Therefore, it can be stated that the growth rate is independent of thickness for the particular range of 25 to 34 mm. This was mainly due to the presence of fully plane strain conditions for the two specimens.

A second 34 mm thick specimen (S3) was tested under the broad band signal of a band width of 0.32 Hz. The results of this specimen and specimen S2 are shown in Fig. 5. They reveal that crack growth rates for the larger band widths of 15 Hz were higher than those under a frequency range of 0.32 Hz, which implies that the increase in band width enhanced the growth rates. This effect is reversed under constant amplitude loading (6). However, CA data are generally presented in terms of length per cycle. If such data be interpreted in terms of length per unit of time, a similar effect would be observed under CA loading. For example, a growth rate of 10^{-5} mm/cycle for a test at a frequency of 50 Hz would be 5×10^{-4} mm/s. The same growth rate at a frequency of 0.5 Hz is 5×10^{-6} mm/s, which is two orders of magnitude smaller than the 50 Hz result. The low frequency results obtained by Musuva (6) are not more than five times greater than the high frequency results, so the effect presented in Fig. 5 is a realistic result. It is difficult to convert random load data to CA ones, there being no definite way of defining cycles within variable amplitude-time histories.

To examine the influence of spectrum shape, a second 25 mm thick specimen (S4) was tested under triple-peaked spectrum loads with a frequency range of 0.32 Hz. The crack propagation data for specimens S4 and S3 are shown in Fig. 6. The crack growth rates for specimen S4 were higher than those for S3, although the mean and rms of the bending stresses were kept constant. The probability density function for the two signals were approximately normal (Gaussian), but the crest factor (or clipping ratio), defined as P_{max}/P_{rms}, was not the same. Smith (4) concluded that such effects are dependent on the level of K. At low K levels, the plastic zones are small and the overload effects due to large peaks would not cause drastic changes in the size of plastic zones. Overloads contribute towards crack growth; hence, crack propagation at low K levels is faster under random load than at CA loading. For large K, the plastic zone size increases significantly with the overloads, and crack growth retardation would therefore occur. The growth rates at high K levels are larger under CA loading compared with variable amplitude loading. It is possible that when the values of K under study are small, the growth rates due to the BP spectrum will be larger as it has a higher crest factor. It can be stated that at low frequencies, the BP spectrum enhances crack growth rates.

Finally, a third 25 mm thick specimen (S5) was tested under a broad band signal of band width of 15 Hz at a Q factor of 8. The results from this specimen and S1, which was loaded with a Q factor of 12, are illustrated in Fig. 7. Under CA and random loading, the increase in mean stress enhances the crack propagation rate. This same effect is observed in Fig. 7. The mean stress effect is more significant in cases of random loading. The mean stress enhances the maximum stress intensity factor levels which control plastic zone size, or open up the crack mouth. The latter situation is detrimental under low frequency loading in adverse environmental conditions.

CONCLUSIONS

The linear elastic fracture mechanics approach was applied to fatigue data obtained during the course of this study to relate crack growth rates at depth and at the surface tips of semi-elliptical surface cracks to the corresponding rms of the stress intensity factor, K_{rms}, of plate bend specimens of BS4360-50D structural steel. It was concluded that:

1. Within the range 25 to 34 mm, the growth rates are indepenent of thickness.
2. Increasing the band width enhances crack growth rates under broad band signals.
3. At the low frequency range of 0.32 Hz, which is relevant to the wave-loads and dynamic response of oil platforms, the triple-peaked spectrum loadings are more detrimental to the crack propagation behaviour of steel than to the broad band loads.
4. Increases in mean stresses reduce the fatigue crack resistance of steel.

REFERENCES

(1) Paris, P.C., and F. Erdogan (1963). A critical analysis of crack propagation laws. J. Basic Eng., Trans. ASME, Series D, 85, 528-534.

(2) Scott, P.M., and T.W. Thorpe (1981). A critical review of crack tip stress intensity factors for semi-elliptic cracks. Fatigue of Engineering Materials and Structures, 4 (4), 291-309.

(3) Roberts, R., and F. Erdogan (1967). The effect of mean stress on fatigue crack propagation in plates under extension and bending. J. Basic Eng., Trans. ASME, 89, 885-892.

(4) Smith, S.H. (1966). Random loading fatigue crack growth behaviour of some aluminium and titanium alloys. ASTM STP 404, 74-100.

(5a) Musuva, J.K., and J.C. Radon (1981). Threshold of fatigue crack growth in a low alloy steel, in Advances in Fracture Research, 3, 1365-1372, ICF5, Pergamon Press.

(5b) Ritchie, R.O. (1977). Near threshold fatigue crack propagation in ultra-high strength steel: Influence of load ratio and cyclic strength. J. Eng. Materials and Technology, Trans. ASME, 195-204.

(6a) Musuva, J.K., and J.C. Radon (1979). The effect of stress ratio and frequency on fatigue crack growth. Fatigue of Engineering Materials and Structures, 1, 457-470.

(6b) Musuva, J.K., and J.C. Radon (1979). Size effects and the J-integral approach to low cycle fatigue crack growth. Proc. Int. Symp. Low Cycle Fatigue Strength and El-plastic Behaviour of Materials, DMW, Stuttgart, 479-494.

(7) Hibberd, R.D., and W.D. Dover (1977). The influence of mean stress and amplitude distribution on random load fatigue crack growth. Eng. Fract. Mech., 9, 251-263.

(8) Dover, W.D., and N.F. Boutle (1978). The influence of mean stress and thickness on the fatigue crack growth behaviour of aluminium alloy BS2271. J. Strain Anal., 13, 129-139.

(9) Hibberd, R.D., and W.D. Dover (1977). The influence of a seawater environment on random load fatigue crack growth in two low alloy steels. Proc. I. Mech. E., 145-160.

(10) Gray, R.M., B. Berge, and A.M. Koehler (1975). Dynamic analysis of the North Sea Forties Field platform. Offshore Technology Conference, Paper No. OTC 2250.

TABLE 1 Test Programme Plan

Specimen Code	Thickness (mm)	Width (mm)	Load Signal (spectrum)	Frequency Bandwidth (Hz)	Q
S1	25	120	BB	0 - 15	12
S2	34	100	BB	0 - 15	12
S3	34	100	BB	0 - 0.32	12
S4	25	120	BP	0 - 0.32	12
S5	25	120	BB	0 - 15	8

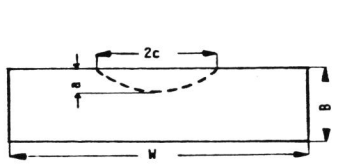

FIG. 1 SPECIMEN CROSS SECTION, a = 2.7 mm, 2c = 27 mm.

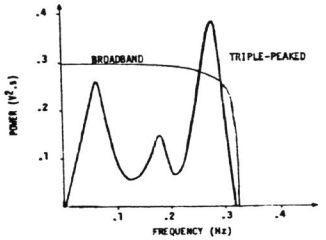

FIG. 2a POWER SPECTRAL DENSITY FUNCTION FOR THE BROADBAND AND TRIPLE-PEAKED SIGNALS.

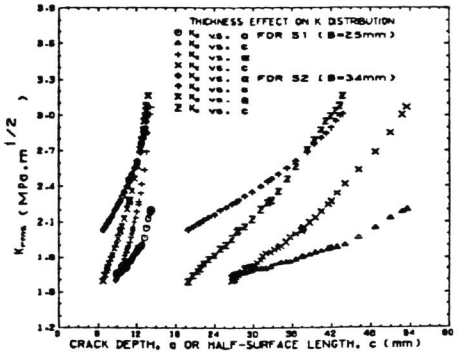

FIG. 3 K_{rms} vs. CRACK DIMENSIONS FOR SPECIMENS S1 AND S2.

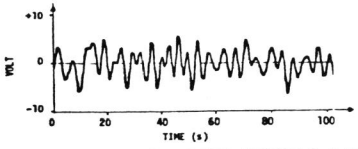

FIG. 2b A RECORD OF TRIPLE-PEAKED SIGNAL (BANDWIDTH 0 - 0.32 Hz).

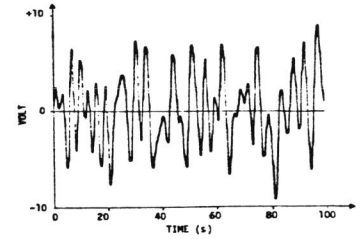

FIG. 2c A RECORD OF BROADBAND SIGNAL (BANDWIDTH 0 - 0.32 Hz).

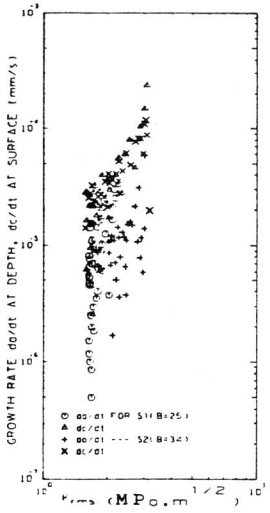

FIG. 4 CRACK GROWTH RATE vs. CORRESPONDING K_{rms} FOR S1 AND S2 (THICKNESS EFFECT).

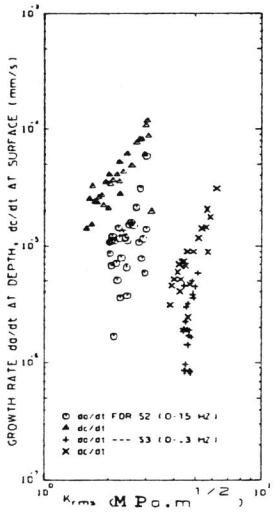

FIG. 5 CRACK GROWTH RATE vs. CORRESPONDING K_{rms} FOR S2 AND S3 (BANDWIDTH EFFECT).

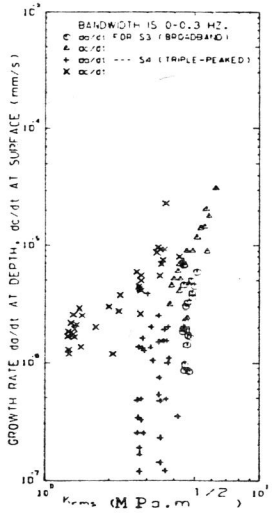

FIG. 6 CRACK GROWTH RATE vs. CORRESPONDING K_{rms} FOR S3 AND S4 (SPECTRUM EFFECT).

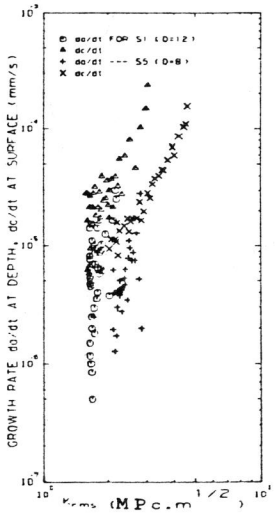

FIG. 7 CRACK GROWTH RATE vs. CORRESPONDING K_{rms} FOR S1 AND S5 (MEAN STRESS EFFECT).